

# Multiresolution Modeling of the Dynamic Loading of Metal Matrix Composites

RÉMI DINGREVILLE,<sup>1,2</sup> JOSHUA ROBBINS,<sup>1</sup> and THOMAS E. VOTH<sup>1</sup>

1.—Sandia National Laboratories, Albuquerque, NM 87185, USA. 2.—e-mail: rdingre@sandia.gov

The mechanical behavior of metal matrix composites (MMCs) varies significantly under rapid straining as compared to quasi-static loading and is often dominated by underlying microstructural features (grain structure, porosity, inclusions, and defects). Analysis of the behavior of MMCs under dynamic loading requires theoretical and experimental approaches that integrate the strain rate and microstructural effects. In this article, we introduce a multi-resolution modeling capability for studying nonlinear planar wave propagation in heterogeneous materials with an application to MMCs. This framework is based on direct numerical simulation (DNS) and compared to an upscaled microcontinuum model. The DNS explicitly accounts for microstructural features characterizing the materials and is based on a combination of a crystal plasticity formulation for the behavior of the host matrix and the Johnson–Holmquist model for the particulate reinforcements. The nonuniformity of the wave propagating through MMCs is spatially resolved. The results from the mesoscale DNS are used to inform a microcontinuum model that introduces richer kinematics to account for microstructural features without explicitly modeling them and with far fewer total degrees of freedom. A quantitative comparison of the reduced degrees of freedom model against DNS is performed and enables us to draw conclusions on the predictive capability of the microcontinuum model to study the dynamic response of heterogeneous materials.

## INTRODUCTION

Metal matrix composites (MMCs) are produced by combining a base metal (such as Al or Ti) or a metallic alloy (such as Ni alloys) with another phase (often nonmetallic) in order to create a novel material with improved mechanical performance compared to conventional materials and to reduce life-cycle costs through enhanced thermomechanical stability and weight reduction.<sup>1–3</sup> MMCs are generally categorized by the characteristics of their reinforcement: particle-reinforced MMCs (e.g., SiC or B<sub>4</sub>C), short fiber- or whisker-reinforced MMCs (e.g., Al<sub>2</sub>O<sub>3</sub>), and fiber or layered MMCs (e.g., C or W). Motivated by technical challenges in processing such composites and tailorability of their properties, and due to the wide range of applications of these materials in advanced military systems (e.g., lightweight armor materials) and in the automotive and aerospace industries (e.g., impact shields, crash-tolerant structures) for example, MMCs and their

thermomechanical performance have been the subject of much research in the late 1980s and early 1990s.<sup>4–10</sup>

This class of materials is often subjected to high-strain-rate deformation, such as in the case of penetration of a projectile in an armor or the impact of an object on aerospace structures, and while showing good performance under such conditions, the mechanical behavior of MMCs varies significantly under rapid straining as compared to quasi-static loading. This behavior is often dominated by underlying microstructural features (grain structure, porosity, shape and spatial distribution of reinforcements, and volume fraction of reinforcements).<sup>11–15</sup> However, despite the great interest in MMCs and considerable research into the effects of reinforcement type and volume fraction on macroscopic properties such as stiffness, ductility, wear resistance, or thermal conductivity, fewer studies have been conducted to examine the effects of those microstructural details on their dynamic loading

behavior.<sup>15–18</sup> The most common and versatile experimental techniques for materials research and characterization under high-strain-rate conditions are uniaxial in character, e.g., high-velocity plate impact and magnetic pulse loading. The assumption of a uniaxial strain condition is valid at the macro-scale, but at the length scale of the microstructure the deformation state is fully three dimensional.<sup>19</sup> Furthermore, the effects of microstructural heterogeneities on the dynamic response of MMCs are particularly pronounced when the scale of the deformation is of the order of the material heterogeneities, which is often the case in dynamic uniaxial experiments. Consequently, there is a critical need for accurate and robust methods for modeling heterogeneous material response at this lower length scale that can account for microstructural effects. Inspired by the work done by Liu and coworkers,<sup>20,21</sup> the current article introduces a multiresolution modeling framework to investigate the dynamic behavior of uniaxially loaded heterogeneous materials, MMCs in particular, by explicitly accounting for the microstructural features (both in the matrix and reinforcements) that influence the dynamic response.

A number of theoretical and numerical investigations has been performed mostly with the intent of predicting the stiffness and strength of a given composite given the properties of the matrix and reinforcement phase.<sup>15,22,23</sup> Analytical studies of the high-strain-rate deformation of particle-reinforced MMCs are based on classic micromechanics schemes and homogenization models (such as mixture models, Mori Tanaka or Hashin–Strickman schemes, etc.). For example, Bao and Lin<sup>24</sup> carried out a micromechanics study to look at the effect of the volume fraction of inclusions on the strain rate dependence of the plastic flow behavior of Al/Al<sub>2</sub>O<sub>3</sub> composites. More recently, Grujicic et al.<sup>25</sup> used a dynamic mixture model in order to investigate the propagation of structured waves within Al/SiC MMCs. Conventional numerical modeling of MMCs is typically conducted at the continuum scale by considering a unit cell model containing a single or multiple idealized reinforcement particle(s) such as a fiber (in the shape of an ellipsoid), a whisker (in the shape of a cylinder), or a particle (idealized as a sphere) embedded in a homogeneous host matrix via computational micromechanics.<sup>15,17,18,26–28</sup> Li and Ramesh<sup>15</sup> for example, performed a parametric study of the influence of particle volume, shape, and aspect ratio on the behavior of particle-reinforced MMCs at a high strain by using an axisymmetric unit cell model with particles treated as elastic ellipsoids or cylinders embedded in an homogeneous viscoplastic matrix. While the simplifications of the microstructural features in these unit cell models may help in reducing the simulation complexity, these models fail to capture the microstructural complexities associated with MMCs' constitutive components such as the inhomogeneous spatial

distributions of particles and their irregular morphology, but also the crystallographic texture and inhomogeneous microstructure (grain size and morphology) of the host matrix itself. Accurate predictions and further understanding of the dynamic behavior for this type of material require an approach that explicitly accounts for realistic microstructures of these composites. For example, Chawla and coworkers<sup>29–31</sup> took a step in that direction by developing microstructure-based finite-element techniques and importing experimentally characterized reinforcements (by serial sectioning, x-ray tomography, or holotomography for example) within a numerical unit-cell framework to study the failure mechanisms of MMCs.

Predicting microstructure–property relationships for the dynamic behavior of MMC materials via direct simulation of its underlying microstructure remains a difficult goal to reach due to the massive disparities in length and time scales. In this article, we present a multiresolution modeling capability for studying the nonlinear planar wave propagation in heterogeneous materials such as MMCs. This framework is based on (I) mesoscale direct numerical simulations (DNS) and (II) an upscaled microcontinuum model. In this article, the term *direct numerical simulation* refers to simulations in which the microstructural topology is explicitly resolved in the spatial discretization. This does not imply that the simulations are considered to be exact solutions to the physical problem, only that an approximation of the microstructure is modeled directly. The mesoscale DNS paradigm used in this work explicitly accounts for microstructural features (grain morphology and crystallographic texture of the matrix, morphology and spatial distribution of the reinforcements) and is based on a combination of a crystal plasticity formulation and Johnson–Holmquist model (JH-1). Nonuniformity of the wave propagating through MMCs is resolved spatially and temporally through these simulations. The results from the mesoscale DNS are then used to inform a microcontinuum model, which introduces richer kinematics to implicitly account for the above-mentioned microstructural features without explicitly modeling them and with far fewer total degrees of freedom than the DNS. The motivation of such an approach is to develop novel multiresolution continuum models of MMCs and relate their microstructure to their structural dynamic performance in a single framework. A quantitative comparison of the reduced degrees of freedom model against DNS is performed and enables us to draw conclusions on the predictive capability of the microcontinuum model compared to fully resolved models to study the dynamic response of heterogeneous materials.

The manuscript is organized as follows. The “[Direct Numerical Simulation of MMCs](#)” section introduces the details of the DNS model used presently. The “[Microcontinuum Model of MMCs](#)”

section describes the details of the microcontinuum model and briefly details the upscaling method between the results obtained from the mesoscale DNS and the microcontinuum model. As an illustration, this work focuses on a prototypical MMC system consisting of an aluminum polycrystalline matrix reinforced with SiC particulates. The “Results and Discussion” section provides a discussion on the main findings of the work for various MMCs (layered and particle reinforced) and recommendations for future investigations.

### DIRECT NUMERICAL SIMULATION OF MMCS

In order to understand and study the dynamic behavior of MMCs, the construction of the multi-resolution continuum model starts at the microstructural level, by treating the material deformation of the MMC matrix with a standard crystal plasticity rate-dependent formulation,<sup>32</sup> while the particle reinforcements are modeled through a JH-1 model.<sup>33</sup>

The foundations of the constitutive model for the MMC matrix assume that the elastoviscoplastic response of single crystals is dominated by slip-deformation mechanisms. Others mechanisms such as twinning, grain boundary sliding, or diffusion are not considered. The total deformation of a single crystal consists of a plastic deformation, elastic lattice rotations, and rigid body rotations. The single-crystal kinematics is described by a multiplicative decomposition of the total deformation gradient  $\mathbf{F}$  into a plastic component  $\mathbf{F}^{\text{plast}}$ , representative of the intervening motion of dislocations on active slip systems leaving the crystal lattice unchanged, and an elastic component  $\mathbf{F}^{\text{elast}}$ , depicting the rotation and elastic stretching of the matrix lattice. For isothermal conditions we have

$$\mathbf{F} = \mathbf{F}^{\text{plast}} \cdot \mathbf{F}^{\text{elast}} \quad (1)$$

Since the dynamic behavior of the polycrystalline matrix is of importance, a rate-form expression of the deformation is used to express the kinematics of the crystalline solid from the kinematic decomposition. The velocity gradient  $\mathbf{L}$  in the current configuration can be written as

$$\mathbf{L} = \dot{\mathbf{F}} \cdot \mathbf{F}^{-1} \quad (2)$$

where  $\dot{\mathbf{F}}$  is the rate of total deformation gradient. Subsequently, the velocity gradient  $\mathbf{L}$  can be additively decomposed into its elastic  $\mathbf{L}^{\text{elast}}$  and plastic  $\mathbf{L}^{\text{plast}}$  counterparts. The plastic velocity gradient  $\mathbf{L}^{\text{plast}}$  is assumed to be solely the result of crystallographic slip over  $S$  potentially active slip systems such that it corresponds to the sum of the plastic shearing rate  $\dot{\gamma}^\alpha$  on  $S$  number of activated slip systems  $\alpha$ ,<sup>34,35</sup>

$$\mathbf{L}^{\text{plast}} = \sum_{\alpha=1}^S \dot{\gamma}^\alpha \bar{\mathbf{m}}^\alpha \otimes \bar{\mathbf{s}}^\alpha, \quad (3)$$

where the plastic velocity gradient is resulting from the dyadic product of the crystallographic slip direction unit vector  $\bar{\mathbf{m}}^\alpha$  and the slip plane normal unit vector  $\bar{\mathbf{s}}^\alpha$  in the intermediate configuration. The rate of plastic deformation gradient  $\dot{\mathbf{F}}^{\text{plast}}$  resulting from crystal slip is governed by

$$\dot{\mathbf{F}}^{\text{plast}} = \mathbf{L}^{\text{plast}} \cdot \mathbf{F}^{\text{plast}} \quad (4)$$

A classic Hookean law gives the constitutive stress–strain relation under isothermal conditions such as

$$\boldsymbol{\sigma}^{\text{PK2}} = \mathbf{C} : \mathbf{E}^{\text{elast}} \quad (5)$$

$$\text{with } \mathbf{E}^{\text{elast}} = \frac{1}{2} \left( \mathbf{F}^{\text{elastT}} \cdot \mathbf{F}^{\text{elast}} - \mathbf{I} \right) \quad (6)$$

where  $\boldsymbol{\sigma}^{\text{PK2}}$  is the second Piola–Kirchhoff stress tensor,  $\mathbf{E}^{\text{elast}}$  is the Green–Lagrange tensorial elastic strain measure,  $\mathbf{C}$  is the anisotropic fourth-order elastic stiffness tensor, and  $\mathbf{I}$  is the second-order identity tensor. The Cauchy stress tensor  $\boldsymbol{\sigma}$  is related to the second Piola–Kirchhoff stress tensor through,<sup>32</sup>

$$\boldsymbol{\sigma} = \left[ \det \left( \mathbf{F}^{\text{elast}} \right) \right]^{-1} \mathbf{F}^{\text{elast}} \cdot \boldsymbol{\sigma}^{\text{PK2}} \cdot \mathbf{F}^{\text{elastT}} \quad (7)$$

The resolved shear stress  $\tau^\alpha$  on slip system  $\alpha$  is defined as

$$\tau^\alpha = \boldsymbol{\sigma} : (\bar{\mathbf{m}}^\alpha \otimes \bar{\mathbf{s}}^\alpha) \quad (8)$$

The flow and evolutionary equations describing the behavior of each individual slip system completes the formulation. The kinetic equation used for the crystallographic slip rate  $\dot{\gamma}^\alpha$  follows a power law viscoplastic flow rule<sup>36</sup> such that

$$\dot{\gamma}^\alpha = \dot{\gamma}_0 \left| \frac{\tau^\alpha}{\tau_{\text{CRSS}}^\alpha} \right|^{1/m} \text{sgn}(\tau^\alpha) \quad (9)$$

where  $\dot{\gamma}_0$  is the reference shearing rate,  $m$  is the rate sensitivity, and  $(\tau^\alpha, \tau_{\text{CRSS}}^\alpha)$  are the resolved shear stress and total slip resistance (or critical resolved shear stress), respectively, on slip system  $\alpha$ . The sign of the resolved shear stress  $\text{sgn}(\tau^\alpha)$  accounts for either positive or negative slip on the system. Hardening of the slip systems assumes that dislocations act as obstacles to dislocation motion and contribute to the total slip resistance according to the Taylor equation.<sup>37</sup> The evolution of the overall resistance to slip,  $\tau_{\text{CRSS}}^\alpha$ , is given by

$$\tau_{\text{CRSS}}^\alpha = \lambda G_{[110]}^b \sqrt{\rho^\alpha} \quad (10)$$

**Table 1. Elastic and viscoplastic parameters for Al matrix**

Property	Symbol	Value
Elastic modulus	$C_{11}$	108.2 GPa
Elastic modulus	$C_{12}$	61.3 GPa
Elastic modulus	$C_{44}$	28.5 GPa
Rate sensitivity	$m$	0.02
Reference shearing rate	$\dot{\gamma}_0$	20 s <sup>-1</sup>
Magnitude of the Burgers vector	$b$	0.286 nm
Initial CRSS	$\tau_{\text{CRSS}}, 0^\alpha$	45.0 MPa
Scaling factor	$\lambda$	0.5
Taylor hardening parameter	$h_1^{\text{KM}}$	$1.07 \times 10^8 \text{ m}^{-1}$
Taylor hardening parameter	$h_2^{\text{KM}}$	27.97

where  $\lambda$  is a statistical coefficient accounting for the deviation from regular spatial arrangements of dislocations,  $b$  is the magnitude of the Burgers vector,  $\rho^\alpha$  is the forest dislocation density for a given slip system  $\alpha$ , and  $G_{[110]}$  is the shear modulus on the [110] plane. Note that the bulk shear modulus  $G$  is instead commonly used in the literature. However, at the grain level, the directional shear modulus seems a better choice due to the local anisotropy of the material.<sup>38</sup> The evolution of the dislocation density is based on the phenomenological approach proposed by Kocks<sup>39</sup> and Mecking and Kocks<sup>40</sup> where dislocation sources and sinks are considered

$$\frac{d\rho^\alpha}{d\gamma^\alpha} = h_1^{\text{KM}} \sqrt{\rho^\alpha} - h_2^{\text{KM}} \rho^\alpha \quad (11)$$

where  $\gamma^\alpha$  is the accumulated slip on the slip system  $\alpha$  and  $(h_1^{\text{KM}}, h_2^{\text{KM}})$  are material hardening parameters. The first term reflects that dislocation storage is inversely proportional to the dislocation mean free path, while the second hardening term describes the annihilation and cross slip of dislocations. Finally, it should be mentioned that the focus of this work is on developing multi-resolution schemes to study the dynamic behavior of heterogeneous materials, rather than the physical models themselves. In other words, the aforementioned flow rule and hardening model are targeted at providing some simple features associated with the hardening of the matrix materials. The elastic constants and hardening parameters introduced in the constitutive model of the section described above are listed in Table 1.

The JH-1<sup>33</sup> is used to describe the SiC particulates behavior. This model incorporates a strength response that possesses both a rate and pressure dependence, and even though this is not the focus of the present study, this model has features that makes it possible to examine the effects of fracture and imperfect interface on loading spreading through a damage parameter  $D$ . The rate dependence of the strength model reads

$$\sigma = \sigma_0 (1 + c_1^{\text{JH}} \ln \dot{\epsilon}^*) \quad (12)$$

where  $\dot{\epsilon}^* = \dot{\epsilon}^{\text{plast}}/\dot{\epsilon}_0$  with  $\epsilon_0$  being a reference strain and  $\epsilon^{\text{plast}}$  being the equivalent plastic strain,  $\sigma_0$  is the material strength at  $\dot{\epsilon}^* = 1$ , and  $c_1^{\text{JH}}$  is a material constant. The pressure-dependent strength for intact ( $D = 0$ ) or partially damaged ( $D < 1$ ) material is given by a bilinear relationship in the pressure/strength space from points  $(P = -P_T, \sigma = 0)$  to  $(P = P_1, \sigma = S_1)$  and from  $(P = P_1, \sigma = S_1)$  to  $(P = P_2, \sigma = S_2)$  followed by a constant strength. The pressure dependence for fully damaged ( $D = 1$ ) material is given by a linear relation in the pressure/strength space from  $\sigma = 0$  to  $\sigma = S_3$  with a slope of  $c_2^{\text{CRSS}}$  followed by a constant strength.

The definition of the damage model describes the fracture behavior of the SiC reinforcements in which the degree of damage is characterized by a scalar metric  $D$ , which varies between 0 (no damage) and 1 (complete damage).  $D$  is defined by

$$D = \frac{\epsilon^{\text{plast}}}{\epsilon^{\text{frac}}} \quad (13)$$

where  $\epsilon^{\text{frac}}$  is the equivalent plastic strain to fracture.

The Mie–Grüneisen equation of state for the volumetric response in the JH-1 is calculated using

$$P = k_1^{\text{JH}} \mu + k_2^{\text{JH}} \mu^2 + k_3^{\text{JH}} \mu^3 \quad (14)$$

where  $(k_1^{\text{JH}}, k_2^{\text{JH}}, k_3^{\text{JH}})$  are material constants and  $\mu = V_0/V - 1$ , with  $V_0$  and  $V$  being the initial and current specific volume, respectively. The material parameters used in JH-1 model are taken from Table 3 in Robbins et al.<sup>41</sup>

A set of different realizations of periodic three-dimensional (3-D) representative microstructures containing Al grains and a given volume fraction of SiC particulate reinforcements was used for the DNS. A typical representative microstructure, illustrated in Fig. 1, was obtained by means of a Voronoi tessellation. Dimensions of the representative volume element (RVE) in physical space is 2.0 mm  $\times$  0.5 mm  $\times$  0.5 mm, resulting in a average grain size of 65  $\mu\text{m}$  and an average reinforcement size of 45  $\mu\text{m}$ . RVEs containing 5% and 10% volume fraction of SiC particulates have been generated and simulated. For each representative microstructure, the crystallographic orientations assigned to each grain in the host matrix is allocated randomly, while perfect bonding between the SiC particulates and Al grains is assumed. The typical mesh for the representative MMC microstructure, selected after a mesh convergence study, comprises an average of 32 million elements, which is equivalent to a 2.5- $\mu\text{m}$  mesh resolution.

This DNS model for MMCs was implemented into Sandia's arbitrary eulerian Lagrangian (ALE) massively parallel ALEGRA code<sup>42,43</sup> and applied to model the dynamic hardening in particle-reinforced MMCs. The ALEGRA framework was used in a pure Lagrangian mode and employs a finite-element

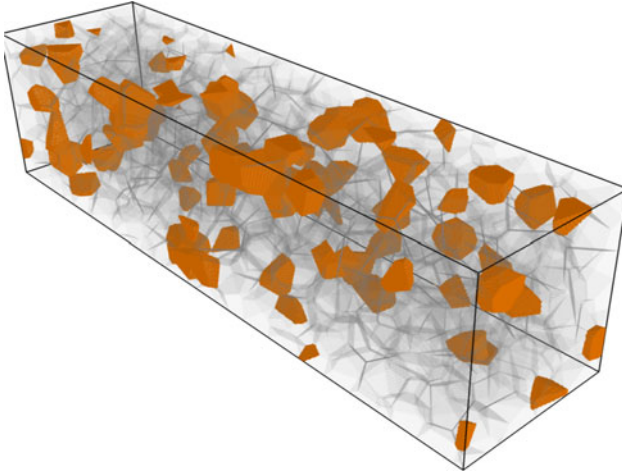


Fig. 1. Typical discretization of Al/SiC MMC. Longitudinal and lateral dimensions are 2.0 mm and 0.5 mm, respectively, and the microstructure is periodic with mesh resolution of 2.5  $\mu\text{m}$ . Aluminum matrix is semitransparent, and SiC reinforcement is opaque.

spatial discretization and an explicit central-difference stepping method in time. The simulations use eight-node, uniform strain, (hexahedral) 3-D isoparametric elements. Hourglass control is used to manage zero-energy modes associated with the uniform strain element. Further details on the formulation of the ALEGRA framework are provided in the technical report by Love and Wong.<sup>42</sup> A set of 12 different 3-D calculations were conducted using 1e4 processor-hours each. Velocity boundary conditions were prescribed as a Gaussian rightward compressive moving pulse of an approximate duration of 200 ns with a half height width of 65 ns at the left end side of the microstructure and with a magnitude of 200 m/s. The lateral sides of the microstructure have periodic boundary conditions. Typical results are presented in Fig. 2 for a microstructure containing 5% of SiC particulates. The input pulse results in a compressive stress wave moving from left to right in the microstructure, which reflects off the free surface after approximately 400 ns producing a release wave. Figure 2 shows grain-scale contour plots of longitudinal velocity at various stages of the wave propagating through the microstructure with sharp contrast between the Al matrix and SiC inclusions. As further illustrated in Fig. 3, which shows the velocity on sample cross sections, spatial variation in the velocity field is produced by the heterogeneity of the material resulting a decidedly multiaxial strain state at this length scale.

## MICROCONTINUUM MODEL OF MMCS

### Multiresolution Continuum Modeling

In an effort to bypass the limitations of computational speed associated with DNS while retaining

microstructural effects, the second step of the construction of the multiresolution continuum model is to pursue the development of an upscaling method informed with details from the mesoscale simulations. Incorporating some effects of characteristic microstructural features of the materials into constitutive modeling is possible via the mechanics of generalized continua. The goal is to endow the continuum with additional degrees of freedom that are supposedly independent from the usual translational degrees of freedom and representative of the microstructure.<sup>44</sup> The article by Germain<sup>45</sup> and the book by Eringen<sup>46</sup> provide detailed reviews of the mechanics of higher order continua. In a microcontinuum model, the underlying microstructure at any material point of the continuum can rotate and deform. In this context, if we consider a continuum  $\mathcal{D}$  as a deformable continuous distribution of material points, each of them is geometrically represented by a point  $M$  and characterized kinematically by a macroscopic and microscopic displacement field. The macroscopic displacement field  $\mathbf{u}$  is defined as  $u_i = x_i - X_i, i = 1 \dots 3$ , where  $x_i$  and  $X_i$  are the coordinates of a material point in the deformed and undeformed reference coordinate system, respectively. The microdisplacement  $\mathbf{u}'$  is defined by its components  $u'_i = x'_i - X'_i$ , where  $x'_i$  are the coordinates of a point  $M'$  belonging to a microvolume  $\Omega(M)$  around  $M$  and measured from the center of mass  $M$  of this microvolume.

Following the development of Mindlin,<sup>47</sup> the balance equations for a microstructured material can be expressed as

$$\nabla \cdot (\boldsymbol{\sigma} + \boldsymbol{\tau}) = \rho \ddot{\mathbf{u}} \quad \text{in } \mathcal{D} \quad (15)$$

$$\nabla \cdot \boldsymbol{\mu} + \boldsymbol{\tau} = \gamma \cdot \mathbf{I}_\mu \quad \text{in } \mathcal{D} \quad (16)$$

where  $\boldsymbol{\sigma}$  is the Cauchy macrostress tensor,  $\boldsymbol{\tau}$  is the relative (interactive) stress tensor,  $\boldsymbol{\mu}$  is the double (micro)stress tensor,  $\gamma$  is the microacceleration,  $\rho$  is the density, and  $\mathbf{I}_\mu$  is the second moment of micro-density. The macrostress can be viewed in a classical manner as the macroscopic average of forces per unit area, while the microstress can be interpreted as a spatial average of the forces arising from the collective nonlocal behavior of the surrounding microstructure.

Concerning the stress and strain measures, we generalize the conventional concept by replacing the Cauchy stress tensor by a generalized stress tensor such that, in the Voigt notation (in which a 9 by 9 tensor can be replaced by a 27-dimensional vector), the generalized stress tensor is expressed as

$$\boldsymbol{\Sigma} = [\boldsymbol{\sigma}, \boldsymbol{\tau}, \boldsymbol{\mu}] \quad (17)$$

Similarly a generalized strain tensor can be expressed as

$$\mathbf{E} = [\boldsymbol{\epsilon}, \boldsymbol{\epsilon} - \boldsymbol{\chi}, \nabla \cdot \boldsymbol{\chi}] \quad (18)$$

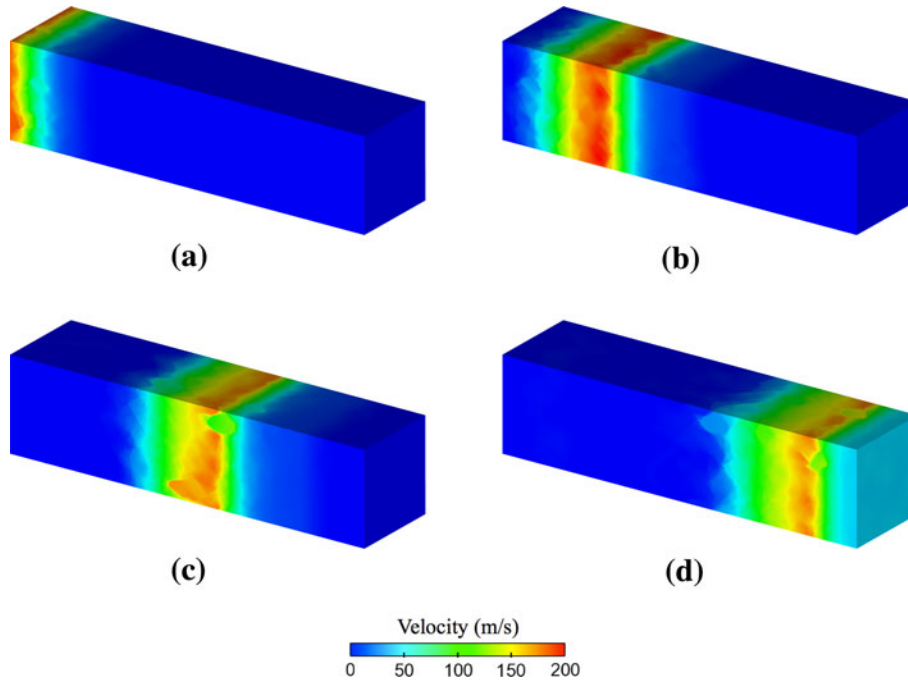


Fig. 2. Comparison of predicted velocity profiles for pulse loading: (a) time =  $8.0 \times 10^{-8}$  s, (b) time =  $1.8 \times 10^{-7}$  s, (c) time =  $2.8 \times 10^{-7}$  s, and (d) time =  $3.8 \times 10^{-7}$  s.

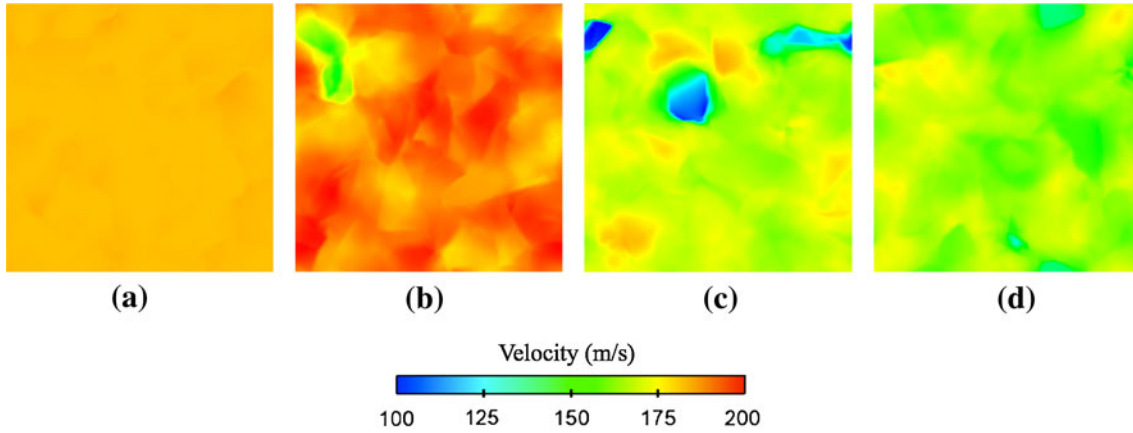


Fig. 3. Comparison of predicted velocity profiles for pulse loading. Cut planes are located at the peak of the pulse. (a) Time =  $8.0 \times 10^{-8}$  s, (b) time =  $1.8 \times 10^{-7}$  s, (c) time =  $2.8 \times 10^{-7}$  s, and (d) time =  $3.8 \times 10^{-7}$  s.

where  $\epsilon = \nabla \cdot u$  is the classical Cauchy strain tensor and  $\chi$  is the microstrain tensor such that the microdisplacement can be approximated by  $u'_i = x'_j \chi_{ji}(x_i, t)$ .

In the elastic regime, the generalized stress and strain are linearly related through a generalized elastic stiffness tensor  $\bar{C}$  that can be written as a block diagonal matrix

$$\bar{C} = \begin{bmatrix} C^0 & A^{0\mu} & 0 \\ A^{0\mu} & C^{0\mu} & 0 \\ 0 & 0 & C^\mu \end{bmatrix} \quad (19)$$

where  $C^0$  is the macroscopic stiffness tensor,  $C^\mu$  is the microscopic stiffness tensor introducing a length scale parameter associated with the microstructure,  $C^{0\mu}$  is a transition stiffness tensor between the macroscopic and microscopic kinematics, and  $A^{0\mu}$  is another coupling term. In this work, we assume that there is no elastic coupling among the macroscales and microscales ( $A^{0\mu} = 0$ ). The tensor  $C^{0\mu}$  is assumed to be associated with a softening/stiffening microstructure such that the resistance to local deformation in the microstructured solid is less/more than the resistance to macroscopic

deformation, i.e.,  $C^{0\mu} = \alpha_1 C^0$ . The microstructural stiffness tensor  $C^\mu$  contains information about the length scale  $\bar{\ell}$  of heterogeneity in the microstructured solid and is taken for simplicity as the second moment of stiffness over the microvolume  $\Omega(M)$ , i.e.,  $C^\mu = \bar{\ell}^2 \alpha_1 C^0$ . Overall, the elastic microcontinuum constitutive model is characterized by two additional constitutive parameters:  $\alpha_1$  and  $\bar{\ell}$ .

The constitutive relation in the plastic regime is based on a classic J2 plasticity model at the macroscopic level, while the microscopic level is assumed to stay elastic. Again, we point out that that the focus of this work is on developing multi-resolution schemes to study the dynamic behavior of heterogeneous materials, rather than the physical models themselves. Therefore, no specific effort has been dedicated in developing a microscale plasticity model. In this context, the plastic potential  $\Phi(\sigma, \kappa)$  is assumed to be solely a function of the Cauchy macrostress tensor and of the equivalent plastic strain  $\kappa$  such that

$$e^p = \dot{\lambda} \frac{\partial \Phi}{\partial \sigma} \quad (20)$$

where  $e^p$  is the plastic deformation,  $\dot{\lambda}$  is a Lagrange plastic multiplier, and  $\partial \Phi / \partial \sigma$  denotes the direction of the plastic flow. As in conventional plasticity, the stress point must remain on the yield surface during plastic deformation, which gives the consistency condition for continuing plastic flow

$$\frac{\partial \Phi^T}{\partial \sigma} \dot{\sigma} + \frac{\partial \Phi}{\partial \kappa} \dot{\kappa} = 0 \quad (21)$$

If we use the gradient to the yield surface  $\mathbf{n}$  according to

$$\mathbf{n} = \frac{\partial \Phi}{\partial \sigma} \quad (22)$$

and the hardening/softening modulus  $h$  as defined in conventional plasticity

$$h = -\frac{1}{\dot{\lambda}} \frac{\partial \Phi}{\partial \kappa} \dot{\kappa} \quad (23)$$

then the consistency equation can be rewritten as

$$\mathbf{n}^T \dot{\sigma} - h \dot{\lambda} = 0 \quad (24)$$

In this article, we apply the strain-hardening/softening hypothesis as defined by

$$\dot{\kappa} = \sqrt{\frac{2}{3}} \dot{e}^p : e^p \quad (25)$$

combined with the Von Mises yield criteria based on the second invariant of the stress tensor.

For the sake of comparison with more classic homogenization methods, the composite macroscale response is also computed by assuming a uniform normal stress in the direction of propagation given the mass fractions  $m_i$  and the constitutive behavior

of the individual materials in a classic rule of mixture manner.<sup>48</sup> When nonlinear compressibility is accounted for, a Mie–Grüneisen equation of state is used. This method is referred to as homogenization in the rest of this manuscript.

### Extracting Microcontinuum Constitutive Relationships from DNS

Before analyzing the dynamic response of MMCs and heterogeneous materials through the current multiresolution continuum model, we will briefly overview the last step of the construction of this model, which consists of extracting the microcontinuum constitutive relationships from the DNS calculations. The goal is achieved here by minimizing the error between the response given by DNS with the one obtained from the microcontinuum model. Note that many strategies can be adopted to optimize and calibrate the parameters from the microcontinuum model to give a best fit to the DNS results, but this discussion is beyond the scope of this article. In this work, in order to calibrate the microcontinuum parameters, we chose to minimize the error between the average velocity given by the DNS with the one obtained from the microcontinuum model. Calibration starts by defining a conventional 3-D RVE and loading with a given compressive pulse input. The average of the velocity over the transverse plane (normal to the propagation direction) is recorded and used to calibrate the microcontinuum model. This is done through a classic multidimensional least-square method such that, if the microcontinuum constitutive model is described by a set of  $n$  parameters  $[\alpha_1, \dots, \alpha_n]$ , then those can be extracted from the DNS simulations through

$$[\alpha_1, \dots, \alpha_n] = \underset{[\alpha_1, \dots, \alpha_n]}{\text{arg min}} \left( \int_t \int_x \int_y \int_z \left( v^{\text{dns}}(x, y, z, t) - v^\mu(x, t; [\alpha_1, \dots, \alpha_n]) \right)^2 dx dt \right) \quad (26)$$

where  $v^{\text{dns}}(x, y, z, t)$  is the velocity obtained from DNS, while  $v^\mu(x, t; [\alpha_1, \dots, \alpha_n])$  is the velocity from the microcontinuum calculation. In the case of our elastic microcontinuum model, calibration is done for the microstructural parameters,  $\alpha_1$  and  $\bar{\ell}$ .

As an illustration of the data extraction methodology, we use a specific example involving a linear elastic layered Al/SiC composite as shown by the schematic in Fig. 4. Each layer of the composite has a thickness of  $\ell = 250 \mu\text{m}$  and is assumed to behave elastically. DNS have been performed on this one-dimensional (1-D) configuration and used as a basis for extracting the microcontinuum constitutive parameters which reduce to two parameters  $(\alpha_1, \bar{\ell})$  in the elastic regime based on Eq. 26. Figure 5a

presents the results of the calibration of the microcontinuum model done for a compressive loading pulse of a given width and height. Based on this calibration, parameters for the microcontinuum model are given by  $\bar{\ell} = 165 \mu\text{m}$  and  $\alpha_1 = 0.0618$ . Note that the microcontinuum length scale  $\bar{\ell}$  is slightly different than the physical length scale  $\ell$  associated with the thickness of the layers of the Al/SiC composite.  $\bar{\ell}$  could be interpreted as a characteristic dispersion length. The parameter  $\alpha_1$  could be interpreted as a softening microstructure such that

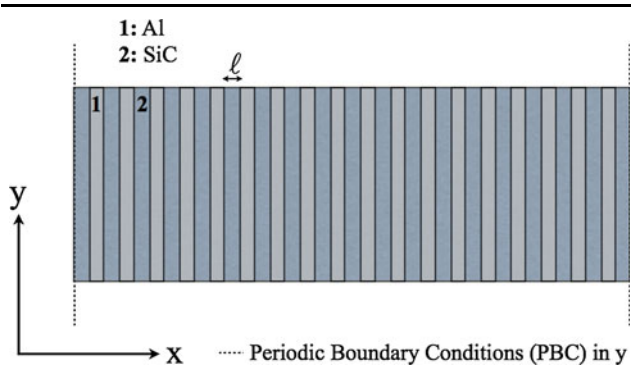


Fig. 4. Schematic of a layered medium used for calibration.

the resistance to local deformation in this microstructured layered composite is less than the resistance to macroscopic deformation. It is also worthwhile to note the qualitative agreement between DNS and the microcontinuum model. In contrast with the results from static homogenization, the microcontinuum model picks up the dispersive character of a loading wave propagating through the medium. In order to verify that these parameters are indeed a reflection of microstructural effects, the same microstructure was subjected to different loading inputs and results were computed keeping the calibrated parameters fixed. Figure 5b, c show the effect of halving and doubling, respectively, the input pulse width while keeping an excellent quantitative comparison with the DNS. Figure 5d illustrates the same comparison for a symmetric impact loading configuration. Again, the agreement between the DNS and the microcontinuum model is preserved. In other words, only a limited number of RVEs and DNS is required to calibrate the constitutive relationships of the aforementioned microcontinuum model. It is also worth pointing out that certain qualitative features given by the DNS results are absent from the classic homogenization such as the attenuation of the peak velocity or the higher frequency ringing after the initial pulse.

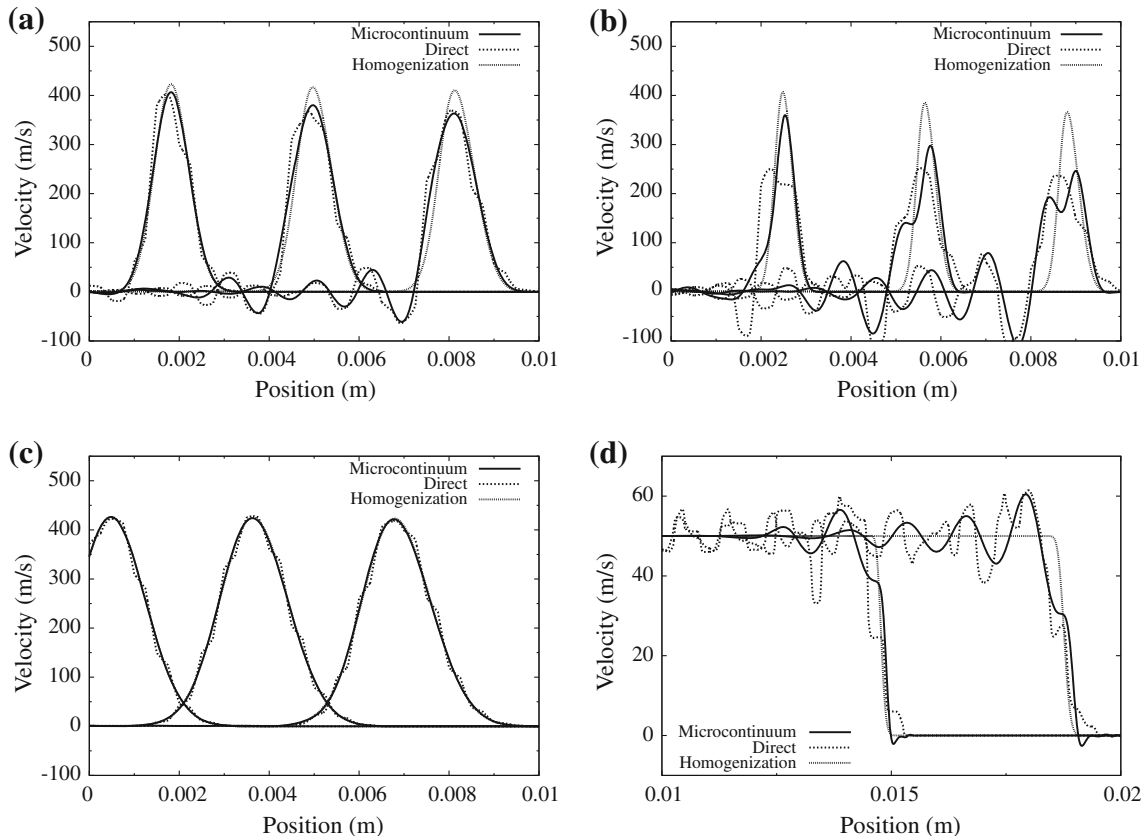


Fig. 5. Comparison of predicted velocity profiles between DNS and the microcontinuum model for a 1-D layered Al/SiC composite in the elastic regime. (a) For a Gaussian input used for initial calibration, (b) for a short pulse loading, (c) for a long pulse loading, (d) for an impact loading.

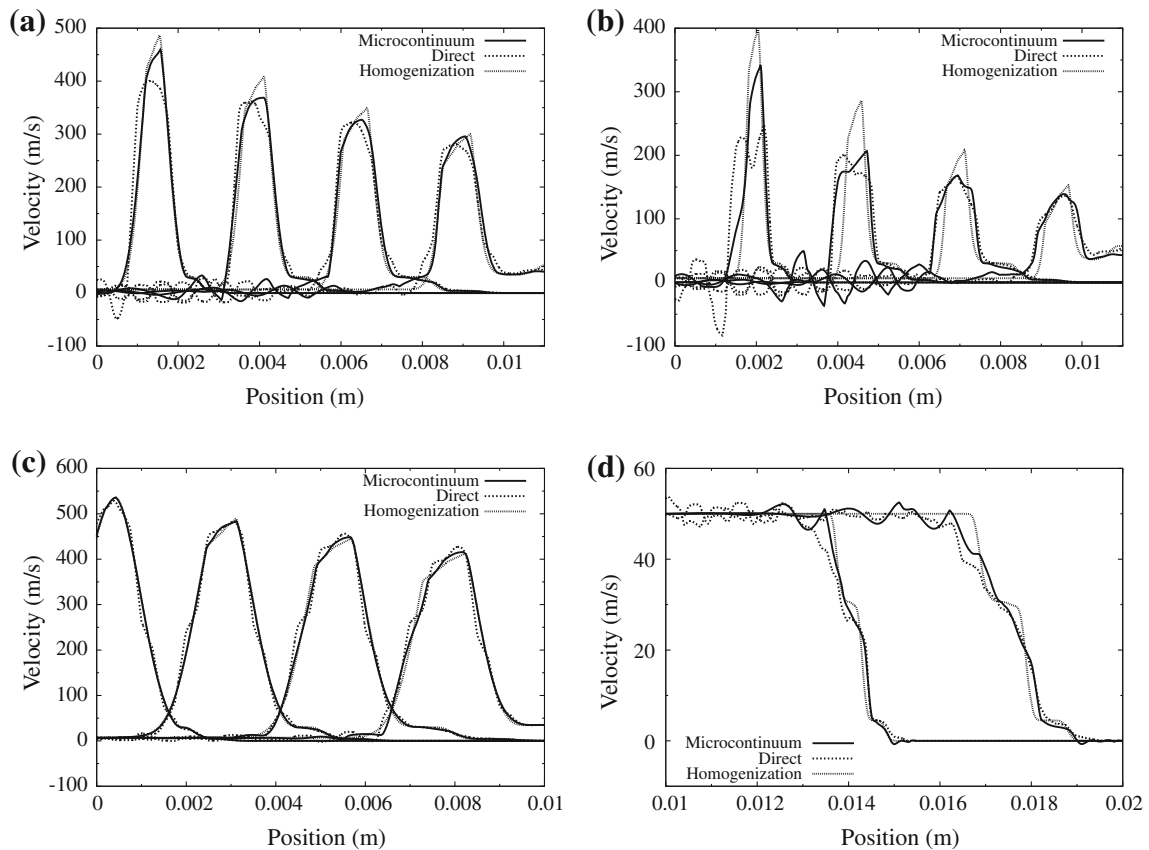


Fig. 6. Comparison of predicted velocity profiles between DNS and the microcontinuum model for a 1-D layered Al/SiC composite in the elastoplastic regime. (a) For a Gaussian input pulse, (b) for a short pulse loading, (c) for a long pulse loading, and (d) for an impact loading.

## RESULTS AND DISCUSSION

The DNS model presented in the “[Direct Numerical Simulation of MMCs](#)” section and the microcontinuum model overviewed in the “[Microcontinuum Model of MMCs](#)” section are first applied to a layered and then to a prototypical particulate-reinforced Al/SiC MMC. The layered composite can be viewed as a 1-D heterogeneous medium while the particulate-reinforced composite is considered as a fully 3-D microstructured medium.

First, we consider the comparison between the results obtained from the microcontinuum model of a nonlinear elastoplastic 1-D layered composite with those obtained by DNS. Following the procedure presented in the “[Extracting Microcontinuum Constitutive Relationships from DNS](#)” section, Fig. 6 presents the comparisons between DNS and the microcontinuum model in the elastoplastic regime. Similar to the purely elastic case, a good agreement is found between DNS and the reduced model. Specifically, the pulse widening and attenuation that is observed in the DNS in the case of a short pulse (see Fig. 6b) is captured by the microcontinuum model. This observation is due to the fact that the length scale associated with the input pulse is of the same order of magnitude as the microstructural

features of the 1-D composite. In contrast, Fig. 6c shows the response to a substantially wider input pulse. In this case, the dispersion of the wave propagating through the microstructured medium is not as pronounced. More interestingly, in the case of an impact loading (see Fig. 6d), both the DNS and microcontinuum model exhibit the continuous broadening of the wave front as it propagates, as opposed to the classic homogenization method, that show two sharp elastic fronts. The results given by the microcontinuum model of wave propagating through the layered composite are consistent with those calculated through DNS but without the associated computational cost. Note that the above features evident in the microcontinuum model and DNS simulations are not captured by the homogenization method because dispersive effects are not present in classic homogenization models.

Second, we examine the case of a three-dimensional particulate-reinforced Al/SiC MMC (see the “[Direct Numerical Simulation of MMCs](#)” section) subjected to a short duration pulse input. Recall that, even though at the continuum scale this is generally considered a uniaxial strain condition, at the scale of the microstructure, the deformation state is fully three dimensional. Ideally, one would have models that capture the dispersion effects

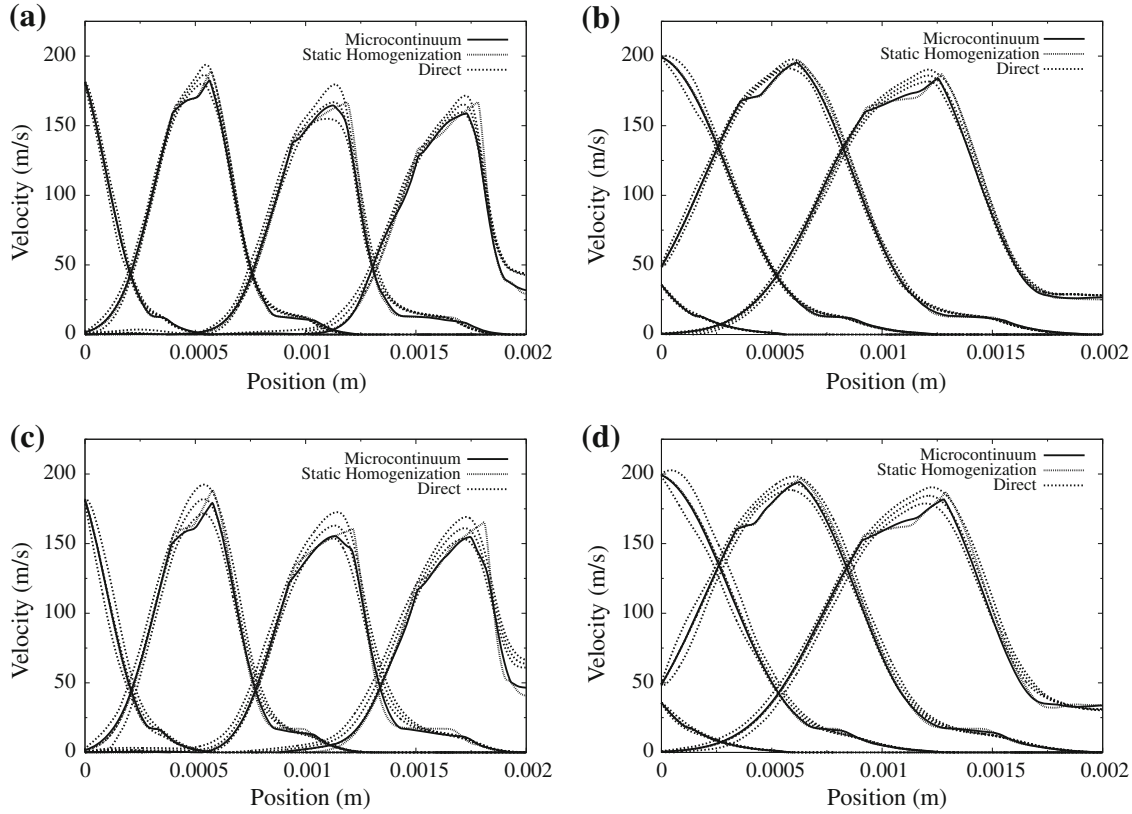


Fig. 7. Comparison of predicted velocity profiles between DNS and the microcontinuum model for a 3-D particulate-reinforced Al/SiC MMC in the elastoplastic regime. The profiles shown of the DNS results are the average of three random microstructural realizations and include an upper and lower envelope that shows the standard deviation in velocity on the transverse plane at the given position. (a) For a Gaussian input pulse with a volume fraction of SiC of 5%, (b) for a long pulse loading with a volume fraction of SiC of 5%, (c) for a Gaussian input pulse with a volume fraction of SiC of 10%, and (d) for a long pulse loading with a volume fraction of SiC of 10%.

associated with the three dimensionality of the microscale response. Figure 7 illustrates how the present multi-resolution scheme constitutes a step in this direction. The DNS incorporates the dispersion behavior of the microstructure directly, so the rate at which the compressive wave steepens due nonlinear stiffening of the volumetric response will be reduced.<sup>49</sup> In the case of the one-dimensional models, the classic homogenization method tends to steepen more rapidly as the wave propagates due to its nondispersive nature; however, the microcontinuum model encapsulates some of the features from the DNS and strikes a balance between the nonlinear volumetric response and dispersion due to the microstructural character of the medium.

The overall trend of the influence of microstructural bias emerging from this multiresolution paradigm illustrates the predictive capability of the microcontinuum model compared to fully resolved models and shows its applicability in the study of dynamic response of heterogeneous materials. Although this approach has shown promise, there are the following outstanding issues warrant further attention:

- In this work, the microscale response was strictly elastic, while the comparison with DNS might

benefit from an elasto-plastic model at this scale. In a separate work,<sup>50</sup> we have examined the impact of microscale plasticity on dispersive behavior, and it is currently under investigation.

- The DNS data that were used in the extraction were an average over the transverse plane. An improvement would be to develop data extraction techniques that incorporate lateral spatial variation present in the three-dimensional DNS into the resulting microstructural parameters, thereby accommodating more information from the DNS.
- While our goal is to develop a lower dimensional model for planar wave propagation, the transition from 3-D DNS to 1-D microcontinuum may incur too much information loss for some applications. Future work will use similar data extraction techniques to inform 3-D microcontinuum models that will be used to quantify the information loss through different levels of abstraction.
- Another issue of considerable interest to the dynamic materials community is the dependence of shock formation rate and eventual thickness on material microstructure. Our results indicate these dispersion effects can be represented by the microcontinuum formulation and can be

improved by refining the physical models both for the DNS and the microcontinuum model.

- In order for the numerical methods in this work to be used with confidence, experimental validation is required. We are currently developing plate impact experiments in well-characterized polycrystalline copper using photon doppler velocimetry for this purpose. Further experiments in MMCs are warranted.

## CONCLUSION

A multiresolution continuum paradigm has been presented to study the dynamic behavior of heterogeneous materials such as MMCs. This framework relies on DNS to spatially resolve the complexity and richness of a wave propagating through microstructured heterogeneous media. The DNS model is based on a combination of a crystal plasticity formulation for the nonlinear behavior of the host matrix and the JH-1 model for behavior of the particulate reinforcements. The results from the mesoscale DNS inform a nonlinear plastic microcontinuum model that introduces richer kinematics to account for microstructural features without explicitly modeling them and with far fewer total degrees of freedom. The microcontinuum model is based on the mechanics of generalized continua and introduces characteristic parameters (characteristic microstructural length scale and microstructural materials parameters for example) arising from the inhomogeneous behavior of the microstructure. These parameters are generally related to microstructural features such as grains and particulate reinforcements.

The resulting multiresolution continuum framework can predict the evolution of continuum fields propagating through a microstructured medium without having to perform the fully resolved microstructural simulations for each loading configuration. Only the DNS used for the calibration of these models are required to determine the microstructural parameters used in the definition of the constitutive behavior of the microcontinuum model.

This multiresolution paradigm has been applied to model the dynamic behavior of layered and particulate-reinforced Al/SiC MMCs. The results from the calibrated microcontinuum model are consistent with those calculated through DNS but without the associated computational cost. Qualitative comparisons of this multiresolution scheme with classic homogenization methods suggest that the result obtained are be more realistic for a wide range of compressive loading inputs. In particular, the dispersive characteristics seem to be better captured when microscale features are in the same order of magnitude as the microstructure. Again, we note that the classic homogenization technique we compare to *cannot* capture these dispersive effects as those physics are *not* present in that model.

Such results show great promise for developing accurate and efficient modeling tools and establish the connection between microstructure and properties. As such, this type of paradigm would be useful in developing new materials with optimal properties for high-strain-rate conditions. For the same reason, such a paradigm would enable and improve our understanding of deformation mechanisms in heterogeneous materials at high strain rates.

## ACKNOWLEDGEMENTS

Sandia is a multiprogram laboratory operated by Sandia Corporation, a Lockheed Martin Company, for the United States Department of Energy, under Contract No. DE-AC04-94AL85000.

## REFERENCES

1. A. Evans, C.S. Marchi, and A. Mortensen, *Metal Matrix Composites in Industry: An Introduction and a Survey Metal Matrix Composites* (Dordrecht, The Netherlands: Kluwer Academic Publishers, 2003).
2. D. Miracle, *Compos. Sci. Technol.* 65 (15–16), 2526 (2005).
3. A. Mortensen and J. Llorca, *Annu. Rev. Mater. Res.* 40, 243 (2010).
4. T. Christman, A. Needleman, and S. Suresh, *Acta Metall.* 37 (11), 3029 (1989).
5. T. Christman, A. Needleman, S. Nutt, and S. Suresh, *Mater. Sci. Eng. A* 107, 49 (1989).
6. J.J. Lewandowski, C. Liu, and W.H. Hunt Jr., *Mater. Sci. Eng. A* 107, 241 (1989).
7. J.K. Shang and R.O. Ritchie, *Acta Metall.* 37 (8), 2267 (1989).
8. J. Llorca, A. Needleman, and S. Suresh, *Acta Metall. Mater.* 39 (10), 2317 (1991).
9. D. Lloyd, *Acta Metall. Mater.* 39 (1), 59 (1991).
10. T.J.A. Doel and P. Bowen, *Composites A* 27 (8), 655 (1996).
11. I.A. Ibrahim, F.A. Mohamed, and E.J. Lavernia, *J. Mater. Sci.* 26, 1137 (1991).
12. R. Vaziri, D. Delfosse, G. Pageau, and A. Poursartip, *Int. J. Impact Eng.* 13 (2), 329 (1993).
13. S.I. Hong and G.T. Gray, *J. Mater. Sci.* 29, 2987 (1994).
14. S. Yadav, D.R. Chichili, and K.T. Ramesh, *Acta Metall. Mater.* 43 (12), 4453 (1995).
15. Y. Li and K.T. Ramesh, *Acta Mater.* 46 (16), 5633 (1998).
16. M. Guden and I.W. Hall, *Mater. Sci. Eng. A* 242 (1–2), 141 (1998).
17. A. Tasdemirci and I.W. Hall, *J. Compos. Mater.* 39 (11), 981 (2005).
18. I. Tirtom, M. Guden, and H. Yildiz, *Comput. Mater. Sci.* 42 (4), 570 (2008).
19. J.R. Asay and L.C. Chhabildas, *High-Pressure Shock Compression of Solids VI: Old Paradigms and New Challenges*, ed. Y. Horie, L. Davison, and N.N. Thadhani (New York: Springer, 2003), pp. 57–119.
20. F. Vernerey, W.K. Liu, and B. Moran, *J. Mech. Phys. Solids* 55 (12), 2603 (2007).
21. C. McVeigh and W.K. Liu, *J. Mech. Phys. Solids* 57 (2), 244 (2009).
22. W.J. Clegg, *Acta Metall.* 36 (8), 2141 (1988).
23. T.G. Nieh, J. Wadsworth, and T. Imai, *Scripta Metall. Mater.* 26, 703 (1992).
24. G. Bao and Z. Lin, *Acta Mater.* 44 (3), 1011 (1996).
25. M. Grujicic, B. Pandurangan, W.C. Bell, C.F. Yen, and B.A. Cheeseman, *Mater. Sci. Eng. A* 528 (28), 8187 (2011).
26. H.J. Böhm, A. Eckschlager, and W. Han, *Comput. Mater. Sci.* 25 (1–2), 42 (2002).
27. J. Segurado, C. González, and J. Llorca, *Acta Mater.* 51 (8), 2355 (2003).
28. J.T. Zhang, L.S. Liu, P.C. Zhai, Z.Y. Fu, and Q.J. Zhang, *Compos. Sci. Technol.* 67 (13), 2775 (2007).

29. N. Chawla, B.V. Patel, M. Koopman, K.K. Chawla, R. Saha, B.R. Patterson, E.R. Fuller, and S.A. Langer, *Mater. Charact.* 49 (5), 395 (2002).
30. N. Chawla, R.S. Sidhu, and V.V. Ganesh, *Acta Mater.* 54 (6), 1541 (2006).
31. J.J. Williams, Z. Flom, A.A. Amell, N. Chawla, X. Xiao, and F. De Carlo, *Acta Mater.* 58 (18), 6194 (2010).
32. F. Roters, P. Eisenlohr, T.R. Bieler, and D. Raabe, *Crystal Plasticity Finite Element Methods* (Weinheim, Germany: Wiley-VCH, Verlag GmbH and Co. KGaA, 2010).
33. G.R. Johnson and T.J. Holmquist, *High Pressure Science and Technology—1993*, ed. S.C. Schmidt, J.W. Shaner, G.A. Samara, and M. Ross (New York: AIP Press, 1994), pp. 1075–1081.
34. R. Hill and J.R. Rice, *J. Mech. Phys. Solids* 20, 401 (1972).
35. R.J. Asaro, *J. Appl. Mech.* 50, 921 (1983).
36. S.I. Hong and G.T. Gray, *Proc. R. Soc. Lond. A* 348, 101 (1976).
37. G.I. Taylor, *Proc. R. Soc. Lond. A* 145 (855), 362 (1934).
38. R. Dingreville, C.C. Battaile, L.N. Brewer, E.A. Holm, and B.L. Boyce, *Int. J. Plast.* 26 (5), 617 (2010).
39. U.F. Kocks, *J. Eng. Mater. Technol.* 98, 76 (1976).
40. H. Mecking and U.F. Kocks, *Acta Metall.* 19 (11), 1865 (1981).
41. J.R. Robbins, J.L. Ding, and Y.M. Gupta, *Int. J. Impact Eng.* 30 (6), 593 (2004).
42. E. Love and M. K. Wong, *Lagrangian Continuum Dynamics in ALEGRA Sandia, Technical Report SAND2007-8104* (Albuquerque, NM: Sandia National Laboratories, 2007).
43. E. Love, G. Scovazzi, and W.J. Rider, *Algorithmic Properties of the Midpoint Predictor-Corrector Time Integrator, Sandia Technical Report SAND 2009-1127* (Albuquerque, NM: Sandia National Laboratories, 2009).
44. S. Forest and R. Sievert, *Int. J. Solids Struct.* 43 (24), 7224 (2006).
45. P. Germain, *SIAM J. Appl. Math.* 25, 556 (1973).
46. A.C. Eringen, *Microcontinuum Field Theories: Foundations and Solids* (New York: Springer, 1999).
47. R.D. Mindlin, *Arch. Ration. Mech. Anal.* 16 (1), 51 (1964).
48. J. Qu and M. Cherkaoui, *Fundamentals of Micromechanics of Solids* (Hoboken, NJ: John Wiley & Sons, Inc., 2006).
49. D. Grady, *J. Mech. Phys. Solids* 46 (10), 2017 (1998).
50. R. Dingreville, J. Robbins, and T.E. Voth, in preparation.